Mid-infrared emission properties of the Tm3+-doped sesquioxide crystals Y2O3, Lu2O3, Sc2O3 and mixed compounds (Y,Lu,Sc)2O3 around 1.5-, 2- and 2.3-μm

R. Moncorgé, Y. Guyot, C. Kränkel, K Lebbou, A. Yoshikawa

Mid-infrared emission properties of the Tm^{3+}-doped sesquioxide crystals Y_2O_3, Lu_2O_3, Sc_2O_3 and mixed compounds $(Y,Lu,Sc)_2O_3$ around 1.5-, 2- and 2.3-µm

R. Moncorgé[1], Y. Guyot[2], C. Kränkel[3], K. Lebbou[2], A. Yoshikawa[4]

1. Centre de recherche sur les Ions, les Matériaux et la Phonique (CIMAP), UMR 6252 CNRS-CEA-ENSICaen, Université de Caen, 6 Boulevard du Maréchal Juin, 14050 Caen Cedex 4, France
2. Institut Lumière Matière (ILM), UMR5306 CNRS, Université de Lyon 1, Campus LyonTech - La Doua, France Bâtiment Kastler, 10 rue Ada Byron, 69622 Villeurbanne, France
3. Zentrum fur Lasermaterialien - Kristalle, Leibniz-Institut fur Kristallzuchtung, Berlin 12489, Germany
4. Institute of Multidisciplinary Research for Advanced Materials (IMRAM), Tohoku University, Sendai, 980-8577, Japan

1. Introduction

Diode-pumped Tm^{3+}-doped sesquioxides Y_2O_3, Lu_2O_3 and Sc_2O_3 [1, 2] have already shown their interest for highly efficient, compact and high power laser systems operating around 2 µm ($^3F_4 \rightarrow {}^3H_6$ Tm^{3+} emission transition) due to a combination of favorable spectroscopic and thermo-mechanical properties: broad and intense absorption and emission bands favorable for diode-pumping and short-pulse laser generation, high crystal hardness, Young modulus and a thermal conductivity favorable for high power laser operation. Several papers were also published concerning the 2 µm emission properties of mixed compositions like $LuScO_3$ [3-6] and $LuYO_3$ [7-10] because of their even broader optical bands and thus more favorable conditions for the generation of ultra-short pulses.

Tm^{3+}-doped materials can also lead to interesting laser emission transitions (see in Fig. 1) around 1.5 µm ($^3H_4 \rightarrow {}^3H_6$) and 2.3 µm ($^3H_4 \rightarrow {}^3H_5$) provided that the host material is characterized by a relatively low maximum phonon frequency allowing for reduced non-radiative multiphonon relaxations, thus high emission quantum efficiencies, and by a relatively low dopant concentration to avoid detrimental quenching of the $^3H_4$ emitting state via inter-ion cross-relaxation energy transfer processes. This has been known since a long time and extensively analyzed and demonstrated in recent years with the well-known fluoride crystals $LiYF_4$ [11-21] and KY_3F_{10} [16, 22, 23] as well as ZBLAN glass [24, 25] with maximum phonon energies (expressed in wavenumbers) of about 430 cm^{-1} [26], 495 cm^{-1} [27] and 500 cm^{-1} [28], respectively, and the $YAlO_3$ oxide crystal [29, 30] with a maximum phonon energy of 552 cm^{-1} [31].

As a matter of fact, Tm^{3+}-doped sesquioxides Y_2O_3, Lu_2O_3 and Sc_2O_3, with maximum phonon energies of about 592, 612 and 669 cm^{-1}, respectively [32, 33], thus reduced non-radiative multiphonon relaxations between adjacent energy levels such as $^3H_4$ and $^3H_5$ [34], should also present interesting $^3H_4 \rightarrow {}^3H_6$ and $^3H_4 \rightarrow {}^3H_5$ emission around 1.5 and 2.3 µm. Preliminary results were already published in the past in the case of Tm^{3+}-doped Y_2O_3, but only around 1.5 µm [35], but nothing can be found in the published literature concerning the 2.3 µm emission in this material and concerning the 1.5 and 2.3 µm emission in the other compounds.

Therefore, the present article aims at presenting a complete investigation of the spectroscopic properties of these three important Tm^{3+}-doped crystalline materials and of their mixed compounds $LuScO_3$, $LuYO_3$ and $YScO_3$ in view of their potential for laser operation around 1.5-, 2- and 2.3-µm.

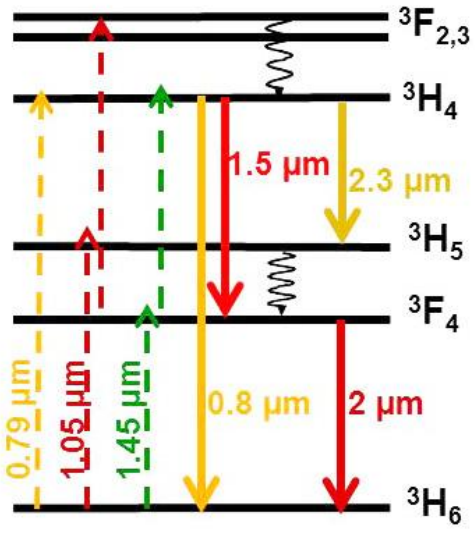

Fig. 1: Energy levels and main near- and mid-infrared excitation (dashed arrows) and emission (full arrows) transitions involved in Tm^{3+}-doped materials (for more complete relaxation and energy transfer schemes, see in [20])

The sesquioxide crystals have the cubic C (bixbyite) structure *(T_h^7, Ia3.* The elementary cell contains 16 formula units with 24 of the 32 cations in sites of C_2 symmetry and the 8 remaining ones in sites of C_{3i} (S_6) symmetry [36, 37]. According to literature, the trivalent rare-earth ions enter these sites in a random manner during the crystal growth. This means that there will be three times as many ions in the C_2 sites as in the C_{3i} sites [38], thus 75% and 25% of the total ion concentration in the respective sites. Since ions in C_{3i} sites exhibit inversion symmetry, only magnetic dipole (MD) optical transitions should be allowed (for example between $^3H_6$ and $^3H_5$ levels of Tm^{3+} ions). For ions in C_2 sites (no inversion center) there are both magnetic- and so-called "forced" electric-dipole (ED) optical transitions.. Of course, vibronic transitions resulting from electron-phonon interaction are always possible in both kinds of sites, but such transitions are generally much weaker than the forced electric-dipole ones. Therefore, it is usually considered that nearly all the spectral lines observed in the absorption spectra of rare-earth doped sesquioxides which have been used to determine the positions of the energy levels, with some exception like the lines corresponding to the $^3H_6$ to $^3H_5$ magnetic-dipole absorption transition, are predominantly due to transitions from ions in sites of C_2 symmetry [34, 38, 39]. Rather contradictorily, however, because the presence of rare-earth ions in the C_{3i} sites were also considered to contribute to the observed line intensities via vibronic and allowed magnetic-dipole processes, the analyses of the absorption spectra made in the past within the Judd-Ofelt (J.O.) formalism [40-43] were performed both by assuming that all the ions contribute to the spectra and without discarding any particular lines in the J.O. treatment.

Consequently, our purpose here will consist in re-analyzing the absorption properties of the six mentioned Tm^{3+} doped sesquioxide compounds within the J.O. formalism, by including or not the $^3H_6 \rightarrow {}^3H_5$ absorption lines in the theoretical treatment, by considering that the totality or only 75% of the Tm^{3+} ions are contributing to the spectra, and also by using revisited transition electric- and magnetic-dipole matrix elements and including specific refractive index variations. Once this being made and the relevance of the obtained results has been established, the most relevant lifetimes and branching ratios will be used to calibrate the emission spectra recorded around 1.5-, 2- and 2.3 µm in cross section units.

Concerning the mixed compounds, the J.O. analysis will be made by using the absorption data available in the literature and the emission spectra will be registered by using compressed powders instead of single crystals.

2. Experimental

The absorption spectra of the available crystals were registered using a Lambda 1050, Perkin Elmer spectrophotometer from 250 to 2000 nm (spectral bandwidth SBW: 0.25 nm up to 850nm, 0.5 nm up to 1000 nm and 1 nm above). The light sources used to excite the samples and register their fluorescence decays and emission spectra were a standard OPO (Optical Parametric Oscillator) pumped by a Q-switched and frequency-doubled Nd:YAG laser and a CW Ti:Sapphire laser, respectively. The emission signals were spectrally analyzed and detected by using an ANDOR Shamrock 500i monochromator equipped with a 600grooves/mm grating blazed at1.9µm and nitrogen cooled InGaAs and InSb photodiodes for the 1.3-1.6 µm and 1.6-2.8 µm spectral ranges, respectively. The wavelength calibration was carried out by using an Hg lamp (Schwabe) and the response of the set-up was further calibrated using a 20 W quartz iodine lamp.

3. Judd Ofelt analysis and discussion on radiative and non-radiative relaxations

The J.O. treatment of the absorption data was performed by considering or not the effect of the $^3H_6 \rightarrow {}^3H_5$ hypersensitive absorption transition around 1200 nm and by considering together the intensities of the overlapping $^3H_6 \rightarrow {}^3F_2$ and $^3F_3$ absorption transitions around 690 nm. The squared reduced matrix elements noted $\langle U^{(t)}_{JJ'} \rangle^2$ with t = 2, 4, 6 used to determine the ED transition strengths $S_{ED}(J, J')$ between multiplets with quantum numbers *J* and *J'* and used for the calculations of the ED spontaneous emission probabilities $A_{ED}(J, J')$ are average values of that found in [29, 44-46]. The wavefunctions used for the calculations of the various MD transition strengths $S_{MD}(J, J')$ and of the various MD spontaneous emission probabilities $A_{MD}(J, J')$ were that given in [47]. Standard expressions for the spontaneous emission probabilities $A_{ED}(J, J')$ and $A_{MD}(J, J')$ versus the transition strengths $S_{ED}(J, J')$ and $S_{MD}(J, J')$ can be found in [46]. The analysis is also performed by using the experimentally measured average absorption wavelengths $\langle \lambda_{abs} \rangle$ and by accounting explicitly for the spectral variations of the refractive indices reported in [48, 49]. The absorption data used in the case of Tm:$LuScO_3$ were those reported in [5] and the J.O. analysis was performed by averaging over the refractive indices of Lu_2O_3 and Sc_2O_3 [49]. In the case of Tm:$LuYO_3$, use was made of the transmittance spectrum reported in [7] and the J.O. analysis was performed by averaging over the refractive indices of Lu_2O_3 [49] and Y_2O_3 [48]. The results are reported in Table 1.

Table 1. Radiative lifetimes τ_r of the $^3F_4$ and $^3H_4$ emitting states and radiative branching ratios $\beta_r(JJ')$ used for calculating the SE cross-sections for the $^3F_4 \rightarrow {}^3H_6$, $^3H_4 \rightarrow {}^3H_5$ and $^3H_4 \rightarrow {}^3F_4$ emission transitions in the considered Tm^{3+}-doped compounds; also indicated the Judd-Ofelt parameters Ω_2, Ω_4 and Ω_6 used to derive these radiative lifetimes and branching ratios and some of the fluorescence lifetimes τ_f reported in the literature and measured at very low dopant concentrations.

Crystal	τ_r, τ_f ($^3F_4$)	τ_r, τ_f ($^3H_4$)	$\beta_r(JJ')$ %			Ω_2, Ω_4, Ω_6	Refs
	ms	ms	$^3H_4 \rightarrow {}^3H_6$,	$^3H_4 \rightarrow {}^3F_4$,	$^3H_4 \rightarrow {}^3H_5$	10^{-20} cm^2	
Y_2O_3	3.61, 3.7	0.64, 0.41	88.09	9.65	2.25	4.07, 1.46, 0.61	[29, 34]
	4.98	0.67	-	-	-	3.17, 1.43, 0.48	[2, 43]
	5.05	0.86	88.18	9.43	2.37	2.51, 0.85, 0.49	*

	3.79	0.65	88.83	8.98	2.18	3.35, 1.13, 0.65	**
Lu_2O_3	5.22, 3.8	0.69, 0.35	-	-	-	2.87, 1.38, 0.45	[2, 42, 50]
	5.08	0.86	88	9.47	2.52	2.29, 0.89, 0.55	*
	3.84	0.65	88.73	8.99	2.28	3.06, 1.19, 0.73	**
Sc_2O_3	6.12, 3.6	0.64	-	-	-	2.58, 0.88, 0.67	[2, 42, 51]
	5.11	0.85	87.73	9.61	2.66	1.98, 0.85, 0.52	*
	3.80	0.65	88.55	9.06	2.38	2.65, 1.15, 0.69	**
$LuYO_3$	6.19	-	-	-	-	2.76, 0.70, 0.53	[8]
	1.3	0.25	91.07	7.17	1.76	5.44, 3.37, 1.57	[9]
	3.89	0.76	87.60	9.60	2.70	3.18, 1.32, 0.41	*
	2.80	0.56	88.10	9.28	2.60	4.10, 1.76, 0.56	**
$LuScO_3$	4.01	0.72	88.3	9.2	2.5	2.43, 1.08, 0.65	[4, 5]
	4.45	0.72	88.55	9.09	2.27	2.54, 0.92, 0.66	*
	3.37	0.55	89.15	8.71	2.10	3.37, 1.22, 0.88	**

Asterisks: Present study without including the $^3H_6$-$^3H_5$ transition and by assuming that all (*) or only 75% (**) of the Tm^{3+} ions are contributing to the observed line intensities**.**

Our results obtained with Tm:Y_2O_3 show that not including the $^3H_6$-$^3H_5$ absorption line intensity in the calculations did not change the values for the radiative lifetimes and the branching ratios significantly. However, it slightly improved the quality of the fit to the data (smaller rms value). On the other hand, by assuming that all the Tm^{3+} ions contribute to the intensities of the absorption lines, the $^3F_4$ and $^3H_4$ radiative lifetimes are found equal to about 5 and 0.86 ms, respectively, and the branching ratios for the $^3H_4 \rightarrow {}^3H_6$, $^3H_4 \rightarrow {}^3H_5$ and $^3H_4 \rightarrow {}^3F_4$ emission transitions around 800 nm, 1500 nm and 2350 nm amount to about 88.2%, 9.4% and 2.4%, respectively. On the contrary, when assuming that only the 75% of the ions which are located in the sites of C_2 symmetry really contribute, it is found $^3F_4$ and $^3H_4$ radiative lifetimes of about 3.8 and 0.65ms and branching ratios of about 88.8%, 9% and 2.2%, thus different lifetimes but similar branching ratios. These last radiative lifetimes are very close to that reported in [34] for Tm:Y_2O_3 where calculations were also probably carried out by assuming that only ions in C_2 sites were contributing to the spectra.

However, if the calculated $^3F_4$ radiative lifetime of about 3.8 ms perfectly agrees with the emission lifetime of 3.7ms measured at a very low dopant concentration of 0.02%Tm [34], one may wonder why our calculations yield a $^3H_4$ radiative lifetime τ_r of about 0.65 ms for a measured emission lifetime τ_f of about 0.41 ms. This comes from the fact that, at room temperature, non-radiative multi-phonon relaxations are non-negligible for level $^3H_4$. Indeed, according to the data reported in Fig. 6 of [34], the rate for non-radiative multiphonon relaxation between adjacent energy levels separated by the energy ΔE would approximately follow the well-known expression:

$$W_{NR} = W_0 \exp(-\alpha \cdot \Delta E) \quad (1)$$

with $\alpha \approx 4.6\times10^{-3}$ cm^{-1} and $W_0 \approx 5\times10^9$ s^{-1}.

Therefore, in the case of Tm :Y_2O_3, an energy gap ΔE between the lowest Stark level of the $^3H_4$ multiplet and the highest Stark level of the $^3H_5$ of about 3639 cm^{-1} [38] would mean a non-radiative decay rate $W_{NR} \approx 267$ s^{-1}. So, according to the expression

$$\frac{1}{\tau_f} \approx \frac{1}{\tau_r} + W_{NR} \qquad (2)$$

it would lead to an effective emission lifetime τ_f of about 0.54 ms, which indeed better fits to the measured emission lifetime.

Namely, the above results show that in the case of Tm:Y_2O_3 the Judd-Ofelt analysis of the absorption spectra must be definitely performed by assuming that only 75% of the ions contribute to the absorption line intensities. This is what will be used for the calibration of the emission spectra in cross-section unit.

In the case of Tm:Lu_2O_3 and Tm:Sc_2O_3, as in the case of the mixed compounds, no specific studies were really performed on Tm^{3+} bulk crystals to decide on the distribution of the dopant ions among the different sites. This site occupancy likely depends on the relative size of the Tm^{3+} and of the Lu^{3+} or Sc^{3+} ions for which they substitute. Therefore, it is probably different for the different compounds. According to some works performed on nano- and micro-crystallites, it would also depend on the crystal growth conditions [52, 53]. Therefore, in the present work, our Judd-Ofelt analysis is carried out, as above, by assuming that 100% or 75% of the Tm^{3+} ions contribute to the absorption line intensities. As in the case of Tm:Y_2O_3, the results (see in Table 1) show that the site occupancy in Tm:Lu_2O_3 and Tm:Sc_2O_3 does change the values of the radiative lifetimes by about 20% but that it only slightly affects the branching ratios. With a maximum phonon energy/wavenumber of about 612 cm^{-1} for Lu_2O_3 and 669 cm^{-1} for Sc_2O_3, instead of 592 cm^{-1} for Y_2O_3, the non-radiative multi-phonon rate contribution to the measured emission lifetimes will be likely stronger in the case Tm:Lu_2O_3 and Tm:Sc_2O_3 than in the case of Tm:Y_2O_3, even for similar energy mismatches. This is probably the reason why (at very low dopant concentration) a smaller $^3H_4$ emission lifetime $\tau_f \approx 0.35$ ms is measured in the case of Tm:Lu_2O_3 [50] and why such a value could be associated as well to a radiative lifetime $\tau_r \approx 0.85$ or 0.53 ms depending on the considered ratio of contributing ions.

As mentioned above, the absorption data used for our J.O. analysis in the case of Tm:$LuScO_3$ and Tm:$LuYO_3$ were those reported in [5] and [7], respectively. As shown in Table 1, our results agree well, in the case of Tm:$LuScO_3$, with that reported in [5]. They strongly differ, however, in the case of Tm:$LuYO_3$, from that reported in [8] and [9]. Indeed, in [8], it is reported a radiative lifetime τ_r = 6.19 ms instead of 3.89 or 2.8 ms (depending on the amount of considered contributing ions). Such a radiative lifetime is certainly too long compared to the radiative lifetimes found in the "parent" compounds Tm:Y_2O_3 and Tm:Lu_2O_3, which do not exceed 5.2 ms, while actually the increased disorder in the mixed compound should rather shorten the lifetime. In the case of [9], it is the reverse since here, a radiative lifetime τ_r = 1.3 ms is found, which is much shorter than it should be.

To complete the above investigation of the non-radiative relaxations affecting the $^3H_4$ and $^3F_4$ emitting levels, fluorescence decay measurements were also performed for all the samples with the same Tm^{3+} dopant concentration of 1 at%, thus ion densities around 3×10^{20} cm^{-3}. Indeed, already at such comparably low dopant concentrations, the $^3F_4$ fluorescence decay curves are nearly but not quite exponential, which is rarely reported in the literature [51]. The authors usually report some average lifetimes without showing the fluorescence decays with a semi-log scale and these average lifetimes are generally shorter than the expected radiative lifetimes. On the other hand, because of more or less efficient cross-relaxation type energy transfers between adjacent Tm^{3+} ions, the $^3H_4$ fluorescence decays are always strongly non-exponential and the time-constant which can be measured is either some average time-constant calculated over the entire fluorescence decay or the time-constant which can be measured in the long-time portion of the fluorescence decay. The results of these measurements are reported in the Figure 2 and Table 2.

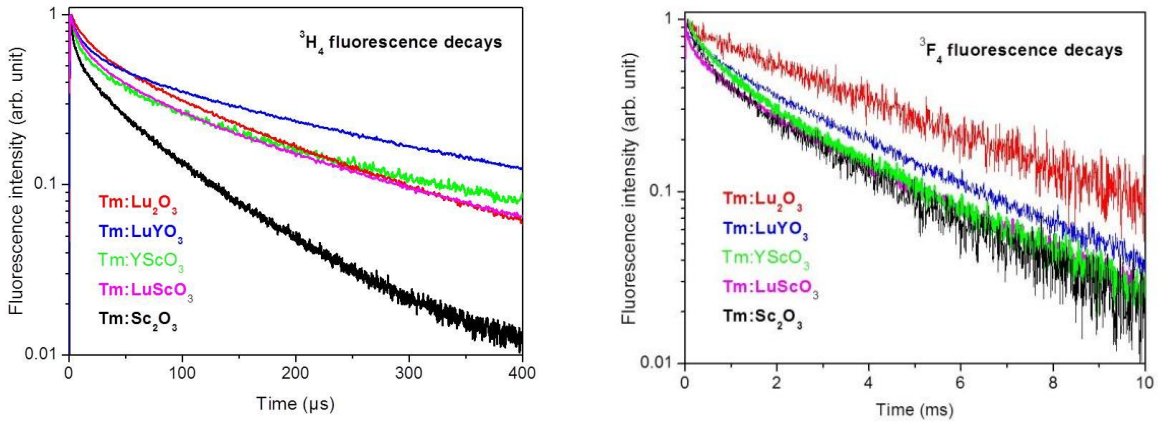

Fig. 2. $^3H_4$ and $^3F_4$ fluorescence decays measured in the 1%Tm-doped compounds after direct excitation at about 795 and 1600nm, respectively.

According to Fig. 2, none of the $^3F_4$ and $^3H_4$ fluorescence decays is entirely exponential. The most exponential behavior is found for the $^3F_4$ emission of Tm:Lu_2O_3 with an average time-constant of about 3.85 ms. In perfect agreement with [51], the more strongly non-exponential decays are found for 1%Tm:Sc_2O_3. According to [51], such non-exponential decays must be assigned to particularly efficient energy migration and direct energy transfers. The other systems exhibit intermediate situations.

Table 2. Fluorescence lifetimes (average and long-time time-constants) measured in the 1%Tm^{3+}-doped compounds

Material	τ_f ($^3F_4$) (ms) average, long-time	τ_f ($^3H_4$) (µs) average, long-time
1%Tm:Y_2O_3[34]	3.7	190
1%Tm:Lu_2O_3	3.85	89, 165
1%Tm:Sc_2O_3	1.6, 2.8	72, 90
1%Tm:$LuYO_3$	2.5, 3.2	75, 230
1%Tm:$LuScO_3$	1.9, 3.3	76, 169
1%Tm:$YScO_3$	1.8, 2.9	78, 171

When comparison is made of these fluorescence lifetimes with those measured at very low dopant concentration and with the calculated radiative lifetimes reported above in Table 1, a number of remarks can be made. First, concerning the non-mixed compounds Tm:Y_2O_3, Tm:Lu_2O_3 and Tm:Sc_2O_3, the $^3F_4$ radiative lifetimes of about 3.8 ms derived by assuming the contribution of only 75% of the ions to the absorption line intensities better fit to the experimental ones. The same good agreement is found for Tm:$LuScO_3$ with a $^3F_4$ radiative lifetime of about 3.37 ms for an experimental one (measured in the long-time portion of the fluorescence decay) of 3.3 ms. The agreement is not so good in the case of Tm:$LuYO_3$ for which we found a (long-time) fluorescence lifetime of 3.2 ms for an expected radiative lifetime of 2.8 ms. It means that the absorption data [7] that were used to derive this radiative lifetime might be not so reliable. This does not seem to be the case for the $^3H_4$ radiative lifetime since about the same value is found for Tm:$LuYO_3$ and Tm:$LuScO_3$.

In conclusion, based on the above considerations, the calibrations of the emission spectra will be performed by assuming that 75% of the Tm^{3+} ions contribute to the line intensities, thus by using the data in Table 1 (as indicated by a double asterisk **), keeping in mind that the obtained cross-section values could be overestimated up to about 25%. However, in the case of Tm:$LuYO_3$, because of not entirely reliable absorption data [7], use will be made of a $^3F_4$ radiative lifetime of 3.2 instead of 2.8 ms. Moreover, in the case of Tm:$YScO_3$ for which no absorption data is yet available, the calibrations will be made by using the β_r/τ_r values found by averaging the β_r/τ_r values of the two other mixed compounds, thus $\beta_r/\tau_r \approx 304\ s^{-1}$ for the $^3F_4$ emission spectrum around 1.9 µm and $\beta_r/\tau_r \approx 162\ s^{-1}$ for the $^3H_4$ emission spectrum around 1.5 µm.

4. Emission cross-section spectra

For crystals with well-defined Stark levels, the cross section of a stimulated emission transition $\sigma_{em,p}^{u\to l}(\lambda)$ between two multiplets *u* and *l* is related to the cross section of the inverse absorption transition $\sigma_{abs,p}^{l\to u}(\lambda)$ by the Einstein "Reciprocity" (RP) (or McCumber) expression which can be written as [54] :

$$\sigma_{em,p}^{RP,u\to l}(\lambda) = \sigma_{abs,p}^{l\to u}(\lambda).\frac{Z_l}{Z_u}.\exp\left[\left(\frac{1}{\lambda_{ZL}}-\frac{1}{\lambda}\right)hc/kT\right] \qquad (3)$$

where *u* and *l* stand for the upper and lower multiplets respectively, *p* is the state of polarization, λ_{ZL} (in nm unit) is the so-called "zero-line" wavelength which corresponds to the energy difference between the lowest sub-levels of each multiplet, $Z_m = \sum_k g_k^m \exp\left(-E_k^m/kT\right)$ is the partition function of the multiplet *m* resulting from the energetic positions E_k^m of the Stark levels of this multiplet, of their degeneracy g_k^m and $hc/kT = 4.8\times10^4$ nm at room temperature.

The detailed energy level positions E_k^m for Tm:Y_2O_3 can be found in [39]. For Tm:Lu_2O_3 and Tm:Sc_2O_3, the Stark level positions can be found in [43] and [51].

According to that data, the calculated zero-line wavelength and partition functions of interest here in this paper are reported in the following Table 3.

Table 3: Zero-line wavelengths and partition functions for the levels involved in the $^3H_4\to{}^3H_6$ (around 800 nm), $^3H_4\to{}^3F_4$ (around 1.45 µm), $^3H_4\to{}^3H_5$ (around 2.35 nm) and $^3F_4\to{}^3H_6$ (around 1.9 µm); data determined for the level positions reported in [39, 43, 51].

Transition	$^3H_4\to{}^3H_6$	$^3H_4\to{}^3F_4$	$^3H_4\to{}^3H_5$	$^3F_4\to{}^3H_6$
	$Z_{^3H_6}$, $\lambda_{ZL}^{^3H_6-{}^3H_4}$ nm	$Z_{^3F_4}$, $\lambda_{ZL}^{^3F_4-{}^3H_4}$ nm	$Z_{^3H_5}$, $\lambda_{ZL}^{^3H_5-{}^3H_4}$ nm	$\lambda_{ZL}^{^3H_6-{}^3F_4}$ nm
Tm:Y_2O_3 [39] $Z_{^3H_4}$ = 3.289	3.847, 796.4	2.795, 1440.7	3.957, 2326.8	1781
Tm:Lu_2O_3[43] $Z_{^3H_4}$ = 2.832	3.899, 796.6	2.688, 1440.1	5.014, 2312.7	1782.8
Tm:Sc_2O_3 [51]	3.458 796.6	2.619, 1440.1	5.889, 2337.5	1782.8

$Z_{^3H_4}$ = 3.031				

When the energy level positions are not quite well defined, an alternative reciprocity method, hereafter called “modified reciprocity” (MRP) method can be used. It consists in calculating the stimulated emission cross section from the absorption one without knowing the respective zero-line wavelengths and partition functions, but introducing the radiative lifetime of the emitting level. Such MRP method is based on the expression [55]:

$$\sigma_{em,p}^{RP,u\to l}(\lambda) = \frac{3}{8\pi c n^2 \tau_r} \frac{\exp(-hc/\lambda kT)}{\sum_p \int \frac{\sigma_{abs,p}^{l\to u}(\lambda)}{\lambda^4} \exp(-hc/\lambda kT)\, d\lambda} \sigma_{abs,p}^{l\to u}(\lambda) \qquad (4)$$

A third method is also currently used, especially when the long-wavelength portion of the absorption cross section spectra is not reported with a high enough signal-to-noise ratio. It is based on the so-called Füchtbauer-Ladenburg (FL) expression:

$$\sigma_{em,p}^{FL,u\to l}(\lambda) = \frac{3\beta_r \lambda^5}{8\pi c n^2 \tau_r} \frac{I_{em,p}^{u\to l}(\lambda)}{\sum_p \int \lambda I_{em,p}^{u\to l}(\lambda)\, d\lambda} \qquad (5)$$

Such a method can be considered in fact as an intermediate method. Indeed, it also uses semi-theoretically derived quantities such as radiative lifetimes and branching ratios, but measured emission intensities noted $I_{em,p}(\lambda)$ instead of absorption spectra. As mentioned above, it is preferred to describe the long-wavelength portions of the emission spectra. However, when it involves transitions with the ground-state of the ions, it can be subject to artefacts on the short-wavelength side due to reabsorption effects, in which case the reciprocity methods lead to better results.

As an example, the absorption and emission cross section spectra obtained using Eq.. (3) and determined assuming that 100% of the Tm^{3+} are contributing to the absorption and emission line intensities, as well as the emission cross section spectra calculated using Eqs. (3), (4) and (5) and assuming the contribution of only 75% of the Tm^{3+} ions, are displayed in the figure 2 in the case of Tm:Lu_2O_3 for the $^3H_6 \leftrightarrow {}^3F_4$ optical transition (for which β_r =1) around 1.9 µm

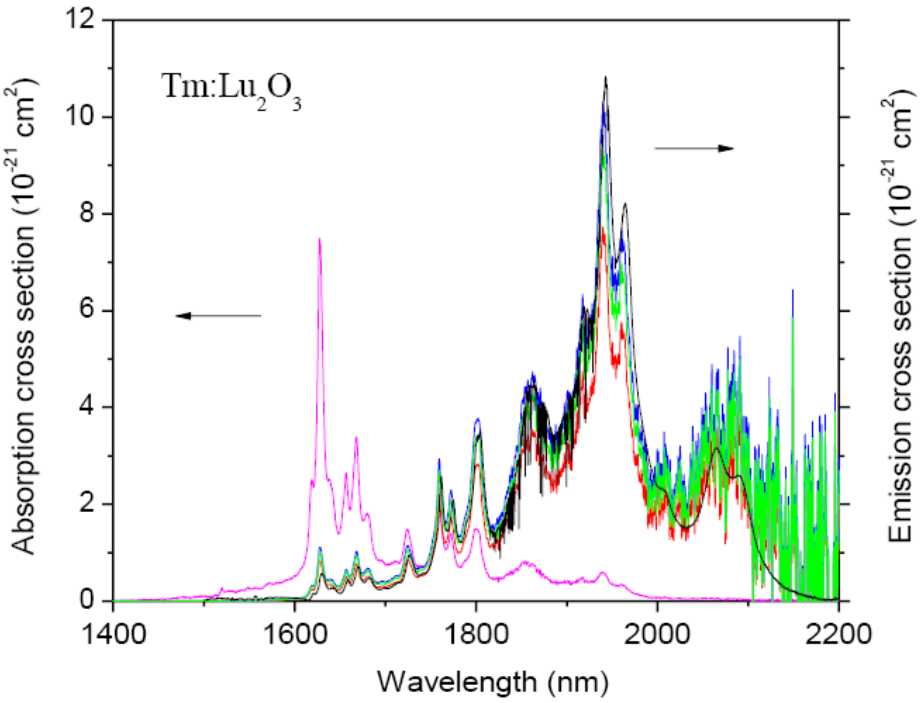

Fig.3. Absorption (magenta) and emission cross spectra (red) of $Tm:Lu_2O_3$ determined around 1.9 µm ($^3H_6 \leftrightarrow {}^3F_4$ optical transitions) by using Expr. (3) and by assuming that 100% of the Tm^{3+} ions contribute to the line intensities; Emission cross section spectra determined by using Eq.. (3) (blue), Eq. (4) (green) and Eq. (5) (black) and by assuming the contribution of only 75% of the Tm^{3+} ions.

These spectra show that the emission cross sections found by assuming the contribution of only 75% of the ions (curves of Fig. 3 reported in green and blue) are increased by approximately 25% compared to what is expected by considering 100% of the ions (curve of Fig. 3 in red), whatever the RP or MRP method which is used. Similar results are obtained in the case of $Tm:Y_2O_3$ and $Tm:Sc_2O_3$, whose spectra can be found in [1, 2].

Figure 4 shows the $^3F_4 \rightarrow {}^3H_6$ emission cross section spectra found around 1.9 µm for the mixed compounds by using the FL method, i.e. Eq. (5), with $\beta_r = 1$ and the radiative lifetimes $\tau_r \approx 3.37$ ms (see in Table 1), 3.2 ms and 3.29 ms, thus $\beta_r/\tau_r \approx 296$, 312 and 304 s^{-1} (see in conclusion of section 3), in the case of Tm-doped $LuScO_3$, $LuYO_3$ and $YScO_3$, respectively. The emission bandshapes for the $Tm:LuScO_3$ and $Tm:LuYO_3$ compounds agree well with that reported in [1, 3, 5, 6] and [8, 9], respectively. Compared with the case of the non-mixed compounds, the spectra are slightly smoother and broader, because of increased structural disorder, and the maxima (see in Table 4) occur at intermediate wavelengths. The emission cross sections found for $Tm:LuScO_3$ are comparable to those reported in [1, 3, 5]. However, the values found in the case of $Tm:LuYO_3$ are almost twice that reported in [8, 9], probably due to inadequate J.O. treatments and cross sections calculations (see in section 3).

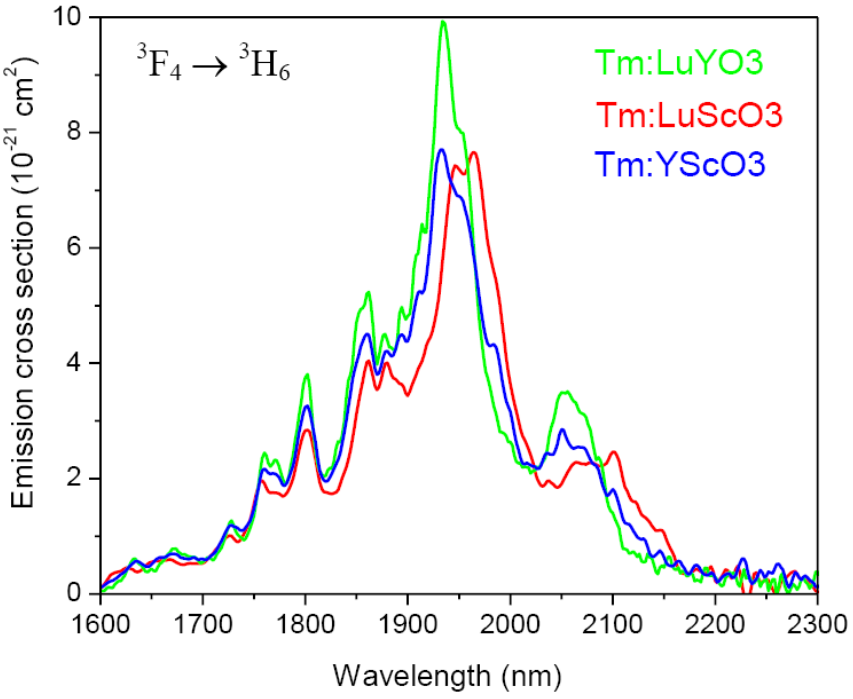

Fig. 4: $^3F_4 \rightarrow {}^3H_6$ emission cross section spectra found around 1.9 µm for the mixed compounds assuming the contribution of 75% of the Tm^{3+} ions and using the FL method with β/τ=312 s^{-1} for $LuYO_3$, β/τ=296 for $LuScO_3$ and the average value β/τ=304 for $YScO_3$.

Table 4. Long-wavelength peak positions found around 2 µm ($^3F_4 \rightarrow {}^3H_6$ emission transition) and 1.5 µm ($^3H_4 \rightarrow {}^3F_4$ emission transition) in the different compounds

Material	$^3F_4 \rightarrow {}^3H_6$ emission peak 1 (nm)	$^3F_4 \rightarrow {}^3H_6$ emission peak 1 (nm)	$^3H_4 \rightarrow {}^3F_4$ emission peak (nm)
1%Tm:Y_2O_3	1932	2051	1550
1%Tm:Lu_2O_3	1945, 1966	2066, 2094	1556
1%Tm:Sc_2O_3	1972, 1988	2115, 2150	1573
1%Tm:$LuYO_3$	1936, 1954	2054, 2074	1552
1%Tm:$LuScO_3$	1948, 1966	2070, 2098	1558
1%Tm:$YScO_3$	1933, 1954	2051	1551

The figures 5 to 8 show the $^3H_4 \rightarrow {}^3F_4$ emission cross section spectra obtained around 1.5 µm by using the FL method and assuming again the contribution of only 75% of the Tm^{3+} ions. As above concerning the mixed compound Tm:$YScO_3$, use was made (according to Table 1) of an average value $\beta/\tau \approx 162$ s^{-1} (166 for Tm:$LuYO_3$ and 158 for Tm:$LuScO_3$). In the case of Tm: Y_2O_3, Tm:Lu_2O_3 and Tm:Sc_2O_3 the figures 5 to 7 also report the $^3F_4 \rightarrow {}^3H_4$ ESA cross section spectra which are obtained by using the RP method, i.e. Eq.. (3).

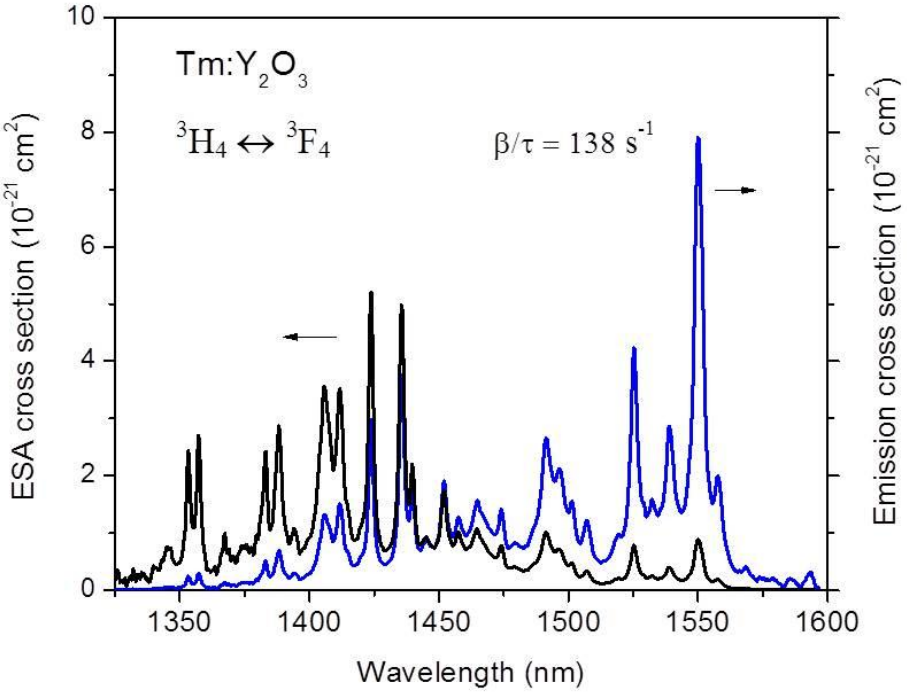

Fig. 5: $^3H_4 \rightarrow {}^3F_4$ emission and $^3F_4 \rightarrow {}^3H_4$ ESA cross section spectra of $Tm:Y_2O_3$ assuming the contribution of 75% of the Tm^{3+} ions.

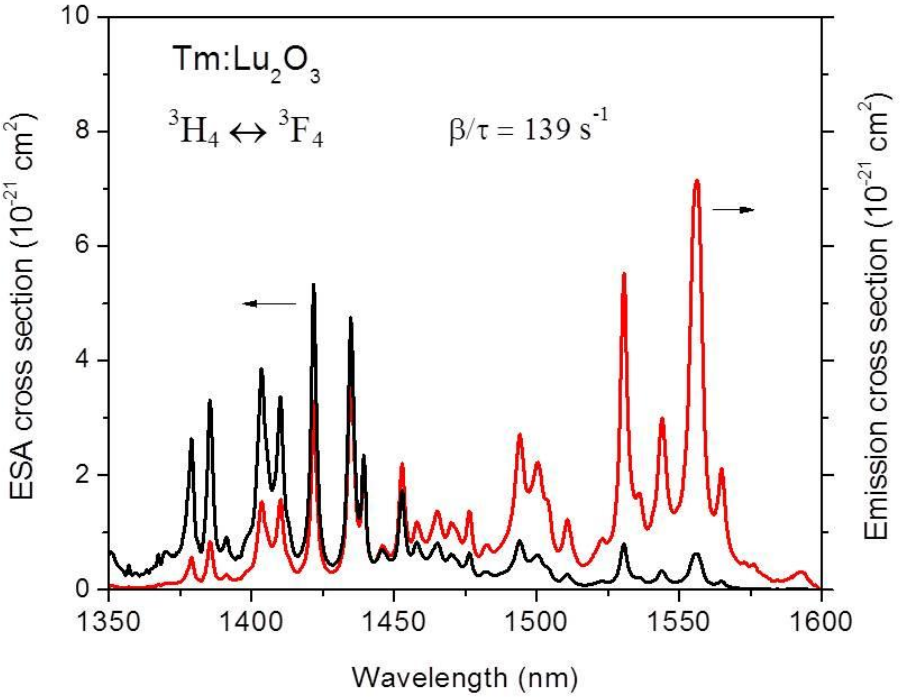

Fig. 6: $^3H_4 \rightarrow {}^3F_4$ emission and $^3F_4 \rightarrow {}^3H_4$ ESA cross section spectra of $Tm:Lu_2O_3$ assuming the contribution of 75% of the Tm^{3+} ions

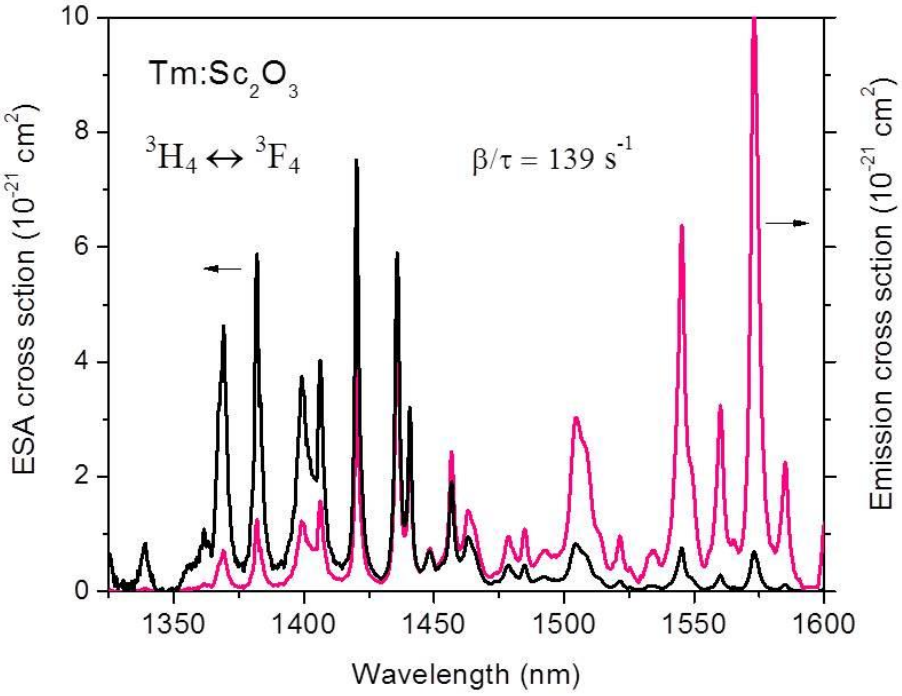

Fig. 7: $^3H_4 \rightarrow {}^3F_4$ emission and $^3F_4 \rightarrow {}^3H_4$ ESA cross section spectra of $Tm:Sc_2O_3$ assuming the contribution of 75% of the Tm^{3+} ions.

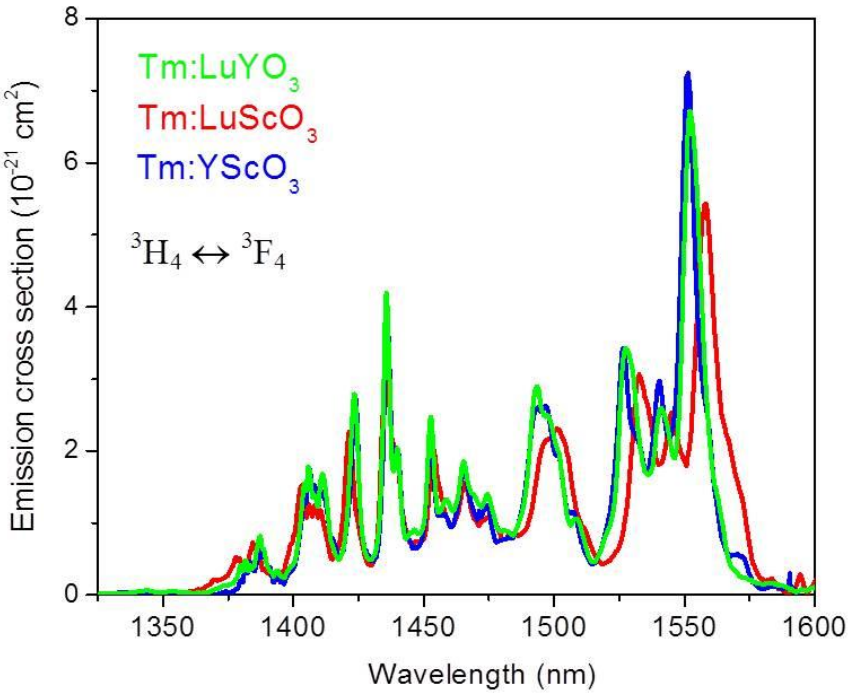

Fig. 8: $^3H_4 \rightarrow {}^3F_4$ emission cross section spectra found around 1.5 μm for the mixed compounds assuming the contribution of 75% of the Tm^{3+} ions and using the FL method with (according to Table 1) β/τ=166 s^{-1} for $LuYO_3$, β/τ=158 s^{-1} for $LuScO_3$ and the average value β/τ=162 s^{-1} for $YScO_3$.

According to these spectra, maximum emission cross sections of about 7 to 10×10^{-21} cm^2 are obtained at about 1550, 1556 and 1573 nm in the case of Tm^{3+}-doped Y_2O_3, Lu_2O_3 and Sc_2O_3, and about 5.5 to 7.5×10^{-21} cm^2 at about 1552, 1558 and 1551 nm in the case of Tm^{3+}-doped $LuYO_3$, $LuScO_3$ and $YScO_3$, respectively. On the other hand, the FWHM of each peak increases from about 4.4 up to about 10 nm when going from pure to mixed sesquioxide compounds. As already noticed for the 2 µm emission, this line broadening explains why the lines appear smoother and less defined. It is caused by the increased structural disorder.

Figure 9 shows the emission cross section spectra associated with the $^3H_4 \rightarrow {}^3H_5$ optical transitions around 2.3 µm and found in the case of Tm^{3+}:Lu_2O_3 and Tm:Sc_2O_3 by using the FL method and assuming again the contribution of only 75% of the Tm^{3+} ions. The spectra for the other compounds were too weak to be measured with a high enough signal-to-noise ratio. The spectra appear as broad, non-structured, bands (probably because of the poor spectral resolution used in the experiments) peaking around 2350 and 2375nm with a FWHM of about 120nm, thus more than twice wider than the emission peaks found around 2050nm (see in Figs 3 and 4.

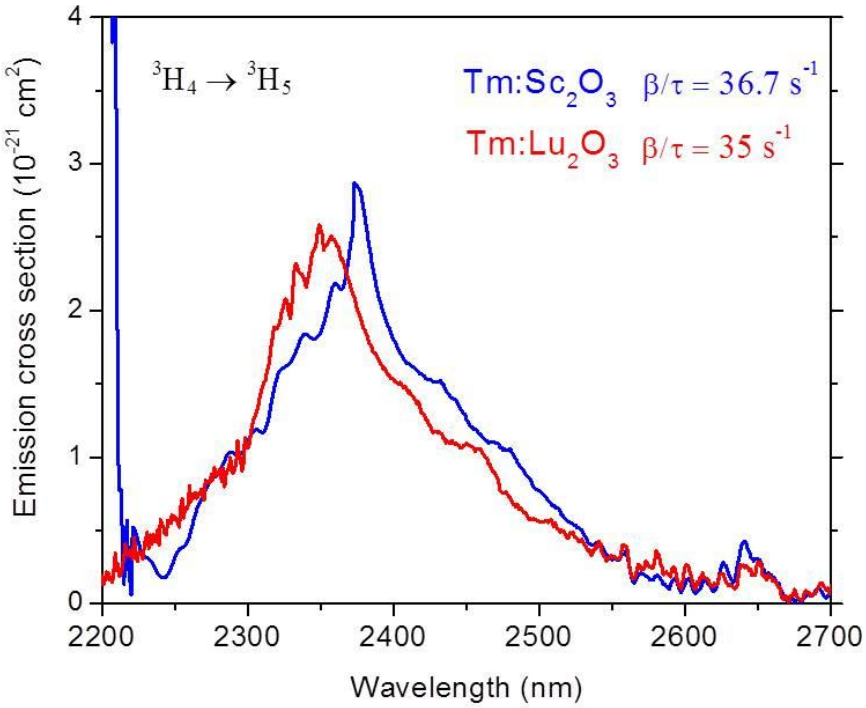

Fig. 9: $^3H_4 \rightarrow {}^3H_5$ emission cross section spectrum of Tm:Lu_2O_3 and Tm:Sc_2O_3 assuming the contribution of 75% of the Tm^{3+} ions.

It is difficult to register good quality spectra in this spectral range for different reasons. It is a question of detectors, which are not as efficient for instance at 2.3µm (InSb photodiode) than at 1.5 µm (InGaAs photodiode), but also and mainly a question of emission intensity. Indeed, such intensity is proportional to the ratio $\frac{\beta_r}{\tau_r}$ and to N^*, the number of excited ions which is itself proportional to a number of parameters according to the expression N^* ; $N_T \phi_{exc} \sigma_{abs} \tau_f$

where N_T stands for the Tm^{3+} dopant concentration, Φ_{exc} for the excitation flux which is used to populate the considered emitting level, and σ_{abs} the absorption cross section at the considered excitation wavelength.
Consequently, when comparison is made between the emission intensities which are expected around 2.3 and 1.9 µm (corresponding to the $^3H_4 \rightarrow {}^3H_5$ and $^3F_4 \rightarrow {}^3H_6$ emission transitions), the intensity ratio, assuming excitation of the $^3H_4$ level, will be roughly given by $\frac{I_2}{I_1} \approx \frac{\beta_{r,2}}{\beta_{r,1}} \frac{\tau_{r,1}}{\tau_{r,2}} \frac{\tau_{f,2}}{\tau_{f,1}}$, where the indices 1 and 2 apply for the 1.9 and 2.3 µm emissions, respectively. Using the data reported in Table 1 and Table 2, thus $\beta_{r,2} \approx 0.02$, $\beta_{r,1} \approx 1$, $\tau_{r,1} \approx$ 3.8ms, $\tau_{r,2} \approx 0.65$ ms, $\tau_{f,1} \approx 3$ ms, $\tau_{f,2} \approx 0.15$ ms (for 1%Tm-doped systems), it is found a ratio of about 0.006, which is indeed pretty low.

5. ESA at the pump and laser wavelengths

Two types of ESA (excited state absorption) transitions are particularily interesting for laser operation of Tm-doped materials at 1.5 and 2.3 µm: the $^3F_4 \rightarrow {}^3F_3$,$^3F_2$ and $^3F_4 \rightarrow {}^3H_4$ transitions which both allow $^3F_4$ energy recycling and two-step excitation pumping of the $^3H_4$ emitting level either via $^3H_6 \rightarrow {}^3H_5$ pump photons around 1.06 µm and rapid $^3H_5 \rightarrow {}^3F_4$ non-radiative multiphonon relaxation or via $^3H_6 \rightarrow {}^3F_4$ pump photons around 1.54 µm, both types of photons being provided by well-spread commercial laser sources. The former ESA transitions take advantage of the strong $^3H_6 \rightarrow {}^3H_5$ absorption peaking around 1.2 µm which extends from about 1.025 to 1.195 µm. The second one is additionally involved in two types of competing cross-relaxation (detrimental) and up-conversion (favorable) energy transfer processes which come into play at medium-high dopant concentrations (generally above 0.5 %Tm ions).

The $^3F_4 \rightarrow {}^3H_4$ ESA transition is just the reverse transition of the above determined $^3H_4 \rightarrow {}^3F_4$ emission occurring around 1.5 µm. The corresponding ESA cross section spectra can thus be easily obtained by using the above defined RP method and the expression:

$$\sigma_{abs,p}^{RP,l\rightarrow u}(\lambda) = \sigma_{em,p}^{u\rightarrow l}(\lambda).\frac{Z_u}{Z_l}.\exp\left[\left(\frac{1}{\lambda} - \frac{1}{\lambda_{ZL}}\right) hc/kT\right] \qquad (6)$$

with $Z_l = Z_{^3F_4}$, $Z_u = Z_{^3H_4}$ (as given in Table 2).

The $^3F_4 \rightarrow {}^3F_2$,$^3F_3$ ESA cross section spectra cannot be obtained in the same way. They can be only obtained experimentally by using a specific pump-probe ESA or ESE (excited state excitation) experiment [56, 57]. As for the previous one, however, an estimation of the integrated absorption cross section can be made by using the J.O. formalism and the parameters reported above and by using the expression [58, for instance]:

$$\int \sigma_{abs,calc}^{l\rightarrow u}(\lambda)d\lambda = \frac{2\pi^2 q^2 \langle\lambda\rangle}{3hc(2J_l+1)\varepsilon_0}\left[\frac{(n^2+2)^2}{9n} S_{ed}^{J_l-J_u} + nS_{md}^{J_l-J_u}\right] \qquad (7)$$

with $$S_{ed}^{J_l-J_u} = \Omega_2.\left[U_{J_lJ_u}^{(2)}\right]^2 + \Omega_4.\left[U_{J_lJ_u}^{(4)}\right]^2 + \Omega_6.\left[U_{J_lJ_u}^{(6)}\right]^2 \qquad (8)$$

and $$S_{md}^{J_l - J_u} = \left(\frac{h}{4\pi m c} \right)^2 \left| \left\langle \varphi_{J_l} \left| \frac{L + 2S}{\mathrm{h}} \right| \varphi_{J_u} \right\rangle \right|^2 \quad (9)$$

where $S_{ed}^{J_l - J_u}$ and $S_{md}^{J_l - J_u}$ stand for the electric-dipole (ed) and magnetic-dipole (md) contributions to the overall strength of the transition, $\frac{2\pi^2 q^2}{3hc\varepsilon_0} \approx 9.59 \times 10^{-2}$, $\left(\frac{h}{4\pi m c} \right)^2 \approx 3.75 \times 10^{-22}$ cm^2 and $\overline{\lambda}$ is given in nm.

Using, as above, average squared reduced matrix elements $\langle U^{(t)}_{JJ'} \rangle^2$ with t = 2, 4, 6 [44, 29, 45 and 46] for the calculation of the electric-dipole transition strengths and the wavefunctions given in [47] for the calculations of the magnetic-dipole ones, it is found:

$$S_{ed}^{^3F_4 - {}^3H_4} \approx 0.1265 \times \Omega_2 + 0.1320 \times \Omega_4 + 0.2147 \times \Omega_6$$
$$S_{ed}^{^3F_4 - {}^3F_3} \approx 0.0025 \times \Omega_2 + 0.0005 \times \Omega_4 + 0.167 \times \Omega_6$$
$$S_{ed}^{^3F_4 - {}^3F_2} \approx 0.2984 \times \Omega_2 + 0.0562 \times \Omega_4 + 0.044 \times \Omega_6$$
$$S_{md}^{^3F_4 - {}^3H_4} \approx 0.139 \times 10^{-20} cm^2$$
$$S_{md}^{^3F_4 - {}^3F_3} \approx 0.154 \times 10^{-20} cm^2$$
$$S_{md}^{^3H_4 - {}^3F_2} \approx 0$$

The results found by using the J.O. parameters derived by assuming that only 75% of the Tm^{3+} ions contribute to the line intensities (see in Table 1) are reported in Table 5. The agreement between the calculated and semi-experimental integrated cross section values for the $^3H_4 \rightarrow {}^3F_4$ ESA transitions around 1.47 µm is quite satisfactory. The integrated cross sections found around 1.06 µm (ESA transition $^3F_4 \rightarrow {}^3F_2$) have the same order of magnitude than the previous ones, which indicate that pumping around these two wavelengths might be good options for future laser experiments.

Table 5. Comparison of the calculated and semi-experimentally determined integrated cross sections for the $^3H_4 \leftrightarrow {}^3F_4$, $^3H_4 \leftrightarrow {}^3F_3$ and $^3H_4 \leftrightarrow {}^3F_2$ ESA transitions of Tm^{3+} ions

Material	Transition	S^{ED}_{calc} $\times 10^{20}$, cm^2	$\langle\lambda_{abs}\rangle$ nm	$\int\sigma_{abs,calc}(\lambda)d\lambda$ $\times 10^{20}$ cm$^2\times$nm	$\int\langle\sigma_{abs}\rangle(\lambda)d\lambda$ $\times 10^{20}$ cm$^2\times$nm
$Tm:Y_2O_3$	$^3F_4 \rightarrow {}^3H_4$	0.712	1475	23.9	20.3
	$^3F_4 \rightarrow {}^3F_3$	0.117	1128	6.0	-
	$^3F_4 \rightarrow {}^3F_2$	1.092	1062	22. 3	-
$Tm:Lu_2O_3$	$^3F_4 \rightarrow {}^3H_4$	0.701	1475	24.5	18.9
	$^3F_4 \rightarrow {}^3F_3$	0.143	1137	6.7	-
	$^3F_4 \rightarrow {}^3F_2$	1.012	1067	21.2	-
$Tm:Sc_2O_3$	$^3F_4 \rightarrow {}^3H_4$	0.635	1479	23.6	18.5
	$^3F_4 \rightarrow {}^3F_3$	0.122	1132	6.5	-
	$^3F_4 \rightarrow {}^3F_2$	0.885	1063	19.3	-

$\int\langle\sigma_{abs}\rangle(\lambda)d\lambda$ is either determined from the corresponding emission spectrum by using the RP method (case of $^3F_4 \rightarrow {}^3H_4$) or from a pump-probe ESA/ESE experiment (case of $^3F_4 \rightarrow {}^3F_3$ and $^3F_4 \rightarrow {}^3F_2$)

6. Conclusion

The spectroscopic properties of the three important Tm^{3+}-doped crystalline materials Y_2O_3, Lu_2O_3 and Sc_2O_3 and of their mixed compounds $LuScO_3$, $LuYO_3$ and $YScO_3$ around 1.5 µm, 1.9 µm and 2.3 µm and corresponding to the three emission transitions $^3H_4 \rightarrow {}^3F_4$, $^3F_4 \rightarrow {}^3H_6$ and $^3H_4 \rightarrow {}^3H_5$, respectively, have been carefully investigated. The absorption data have been re-examined within the formalism of the Judd-Ofelt theory by using the same procedure (revisited ED and MD matrix elements, account of specific refractive index dispersions, elimination of hypersensitive transitions) and by making the assumption of the contribution of only 75% of the active ions, those located in C_2 symmetry sites, to the absorption line intensities. Decay times measurements have been performed and the measured fluorescence lifetimes agreed and therefore re-inforced the above assumption and the derived radiative lifetimes and branching ratios. It also means that making calculations, as it was often made in the past literature, by assuming that 100% of the Tm^{3+} ions are contributing to the observed spectroscopic or laser properties, thus by using the full doping concentration, might be wrong. The above derived radiative lifetimes and branching ratios have been used then to calibrate the various experimentally measured emission spectra in cross section unit. Excited state absorption (ESA) cross section calculations have been finally carried out for the three $^3F_4 \rightarrow {}^3F_2$, $^3F_4 \rightarrow {}^3F_3$ and $^3F_4 \rightarrow {}^3H_4$ ESA transitions of interest around 1.06, 1.13 and 1.47 µm, respectively, and the results concerning the latter been compared with what is expected from the emission cross section spectra determined around 1.5 µm and corresponding to the $^3H_4 \rightarrow {}^3F_4$ reverse transition. These results show that Tm-doped mixed compounds exhibit wider emission bands around 1.5 and 2 µm than in the non-mixed compounds, while keeping comparable emission cross sections. From this point of view, $Tm:LuYO_3$ appears more favorable than $Tm:LuScO_3$ and $Tm:YScO_3$. Short pulse and broad-band laser operation (via Q-switching or mode-locking) of the various systems around 1.55 µm after ESA pumping around 1.47 µm (thus depopulation of the terminal state of the laser transition) might be worth to be tried in the future. However, the results obtained concerning the 2.3 µm emission transition show that it is too weak to compete with other Tm-doped materials like fluorides.

References

1. C. Kränkel, "Rare-Earth-Doped Sesquioxides for Diode-Pumped High-Power Lasers in the 1-, 2-, and 3-μm Spectral Range" IEEE J. Sel. Top. Quant. Electr. **21** (1), 1602013 (2015) and refs therein

2. P. Loiko , P. Koopmann, X. Mateos , J. M. Serres, V. Jambunathan, A. Lucianetti, T. Mocek, M. Aguilo, F. Dıaz, U. Griebner, V. Petrov and C. Kränkel, "Highly Efficient, Compact $Tm^{3+}:RE_2O_3$ (RE = Y, Lu, Sc) Sesquioxide Lasers Based on Thermal Guiding" IEEE J. Sel. Top. Quant. Electr. **24** (5), 160013 (2018) and refs therein

3. P. Koopmann, S. Lamrini, K. Scholle, P. Fuhrberg, K. Petermann, and G. Huber, "Laser Operation and Spectroscopic Investigations of $Tm:LuScO_3$" CLEO/Europe (2011), paper **CA1–4**

4. X. Xu, Z. Hu, D. Li, P. Liu, J. Zhang, B. Xu, and J. Xu, "First laser oscillation of diode-pumped Tm^{3+}- doped $LuScO_3$ mixed sesquioxide ceramic", Opt. Expr. **25** (13), pp 15322-29 (2017)
5. W. Jing, P. Loiko, J. M. Serres, Y. Wang, E. Vilejshikova, M. Aguilo, F. Diaz, U. Griebner, H. Huang, V. Petrov, X. Mateos, "Synthesis, spectroscopy, and efficient laser operation of "mixed" sesquioxide Tm:$(Lu,Sc)_2O_3$ transparent ceramics" Opt. Mat. Expr. **7** (11), pp 4192-4202 (2017)
6. H. Wu, G.H. Pan, Z. Hao, L. Zhang, X. Zhang, L. Zhang, H. Zao, J. Zhang, "Laser-quality Tm:$(Lu_{0.8}Sc_{0.2})_2O_3$ mixed sesquioxide ceramics shaped by gelcasting of well-dispersed nanopowders" J. Am. Ceram. Soc. **102**, pp 4919–4928 (2019)
7. Z. Zhou, X. Guan, X. Huang, B. Xu, H. Xu, Z. Cai, X. Xu, P. Liu, D. Li, J. Zhang, and J. Xu, "Tm^{3+}-doped LuYO3 mixed sesquioxide ceramic laser: effective 2.05 μm source operating in continuous-wave and passive Q-switching regimes" Opt. Lett. **42** (19), pp 3781-84 (2017)
8. D. Li, L. Kong, X. Xu, P. Liu, G. Xie, J. Zhang, J. Xu, "Spectroscopy and mode-locking laser operation of Tm:$LuYO_3$ mixed sesquioxide ceramic" Opt. Expr. **27** (7) pp 24416-25 (2019)
9. G. Chen, S. Li, L. Zhang, X. Tan, W. Deng, M. He, M. Xu, Y. Yang, S. Zhang, Y. Hang, "Growth and spectra of Tm^{3+} doped $LuYO_3$ single crystal for 2 μm lasers" Infrared Phys. & Tech. (2020) doi.org/10.1016/j.infrared.2020.103431
10. Y. Zhao, L. Wang, W. Chen, Z. Pan, Y. Wang, P. Liu, X. Xu, Y. Liu, D. Shen, J. Zhang, M. Guina, X. Mateos, P. Loiko, Z. Wang, X. Xu, J. Xu, M. Mero, U. Griebner, V. Petrov, "SESAM mode-locked Tm:$LuYO_3$ ceramic laser generating 54-fs pulses at 2048 nm" Appl. Opt. **59** (33) pp 10493-97 (2020)
11. R. Allen and L. Esterowitz, "CW diode pumped 2.3 μm fiber laser" Appl. Phys. Lett. **55**, p 721 (1989)
112 R.C. Stoneman, L. Esterowitz, "Continuous-wave 1.50 μm thulium cascade laser", Opt. Lett. **16** (4), pp 232-234 (1991)
13. J. F. Pinto and L. Esterowitz, G. H. Rosenblatt, "Tm^{3+}:YLF laser continuously tunable between 2.20 and 2.46 μm" Opt. Lett. **19** (12), p 883 (1994)
14. A. Diening, P.E.A. Mobert, G. Huber, "Diode-pumped continuous-wave, quasi-continuous-wave and Q-switched laser operation of Yb^{3+},Tm^{3+}:$YLiF_4$ at 1.5 and 2.3 μm", J. Appl. Phys. **84** (11), pp 5900-5904 (1998)
15. A. Braud, M. Fromager, J.L. Doualan, S. Girard, R. Moncorgé, M. Thuau, B. Ferrand , Ph. Thony "Passive Q-switching and wavelength tunability of a diode-pumped Tm:Yb:YLiF laser around 1.5 μm", Opt. Comm. **183**, 175–179 (2000)
16. A. Braud, S. Girard, J. L. Doualan, M. Thuau, and R. Moncorgé "Energy-transfer processes in Yb:Tm-doped KY_3F_{10}, $LiYF_4$, and BaY_2F8 single crystals for laser operation at 1.5 and 2.3 μm" Phys. Rev. B **61**, pp 5280-5292 (2000)
17. P.S.F. de Matos, N.U. Wetter, L. Gomes, I.M. Ranieri and S.L. Baldochi, "A high power 2.3 μm Yb:Tm:YLF laser diode-pumped simultaneously at 685 and 960 nm" J. Opt. A: Pure Appl. Opt. **10**, p 104009 (7pp) (2008)
18. F. Canbaz, I. Yorulmaz and A. Sennaroglou, "2.3-μm Tm^{3+}:YLF laser passively Q-switched with a Cr^{2+}:ZnSe saturable absorber" Opt. Lett. **42** (9), p 1656 (2017)
19. R. Soulard, A. Tyazhev, J.L. Doualan, A. Braud, A. Hideur, M. Laroche, B. Xu, P. Camy, "2.3 μm Tm^{3+}:YLF Mode-locked laser" Opt. Lett**. 42** (18), pp. 3534-3536 (2017)
20. L. Guillemot, P. Loiko, R. Soulard, A. Braud, J.L. Doualan, A. Hideur, R. Moncorgé and Patrice Camy, "Thulium laser at ~2.3 μm based on upconversion pumping" Opt. Lett. **44** (16) pp 4071-4074 (2019)

21. P. Loiko, R. Soulard, L. Guillemot , G. Brasse, J.L. Doualan, A. Braud, A. Tyazhev , A. Hideur, F. Druon, and P. Camy, "Efficient Tm:LiYF4 Lasers at 2.3 μm: Effect of Energy-Transfer Upconversion" IEEE J. Quant. Electr. **55** (6) 1700212 (2019)
22. A. Muti, M. Tonelli, V. Petrov, A. Sennaroglou, "Continuous-wave mid-infrared laser operation of Tm^{3+}:KY_3F_{10} at 2.3 μm" Opt. Lett. **44** (13) pp 3242-3245 (2019)
23. L. Guillemot, P. Loiko, R. Soulard, A. Braud, J.L. Doualan, A. Hideur, P. Camy, "Close look on cubic Tm:KY_3F_{10} crystal for highly-efficient lasing on the $^3H_4 \rightarrow {}^3H_5$ transition", Opt. Expr. **28** (3), pp 3451-3463 (2020)
24. L. Esterowitz, R. Allen, I. Aggarwal, "Pulsed laser emission at 2 μm in a thulium-doped fluorozirconate fibre" Electr. Lett. **24** (17) 1104 (1988)
25. G. Androz, M. Bernier, D. Faucher and R. Vallée "2.3 W single transverse mode thulium-doped ZBLAN fiber laser at 1480 nm" Opt. Expr. **16** (20), pp 16019-16031 (2008)
26. A.M.E. Santo, A.F.H. Librantz, L. Gomes, P.S. Pizani, I.M. Ranieri, N.D. Vieira Jr., S.L. Baldochi, "Growth and characterization of $LiYF_4$:Nd single crystal fibres for optical applications" Journal of Crystal Growth **292** (2006) 149–154
27. M. Chen, P. Loiko, J.M. Serres, S. Veronesi, M. Tonelli, M. Aguilo, F. Diaz, S.Y. Choi, J.E. Bae, F. Rotermund, S. Dai, Z. Chen, U. Griebner, V. Petrov, X. Mateos, "Fluorite-type Tm^{3+}:KY_3F_{10}: A promising crystal for watt-level lasers at ~1.9 μm" J. Alloys Comp. **813** (15) 152176 (2020)
28. B.M. Walsh, N.P. Barnes, "Comparison of Tm: ZBLAN and Tm: Silica Fiber Lasers; Spectroscopy and Tunable Pulsed Laser Operation Around 1.9 μm" Appl. Phys. B **78** (3) pp 325-333 (2004)
29. J. A. Caird, L.G. DeShazer, and J. Nella, "Characteristics of Room-Temperature 2.3-μm Laser Emission from Tm^{3+} in YAG and $YA1O_3$" IEEE J. Quant. Electr. QE **11** (11) pp 874-881 (1975)
30. L. Guillemot, P. Loiko, A. Braud, J.L. Doualan, A. Hideur, M. Koselja, R. Moncorgé, P. Camy, "Continuous-wave Tm:$YAlO_3$ laser at ~2.3 μm" Opt. Lett. **44** (20) pp 5077-5080 (2019)
31. A. Chopelas, "Single-crystal Raman spectra of $YAlO_3$ and $GdAlO_3$: comparison to several orthorhombic ABO_3 perovskites" Phys. Chem. Mineral. **38**, 709 (2011)
32. L. Laversenne, Y. Guyot, C. Goutaudier, M. T. Cohen-Adad, and G. Boulon, "Optimization of spectroscopic properties of Yb^{3+} -doped refractory sesquioxides: Cubic Y_2O_3, Lu_2O_3 and monoclinic Gd_2O_3" Opt. Mater. **16** (4) pp. 475–483 (2011)
33. M. V. Abrashev, N. D. Todorov, and J. Geshev, "Raman spectra of R_2O_3 (R-rare earth) sesquioxides with C-type bixbyite crystal structure: A comparative study" J. Appl. Phys. **116** (10) 103508 (2014)
34. M.J. Weber, "Radiative and Multiphonon Relaxation of Rare-Earth Ions in Y_2O_3", Phys. Rev. **171** (2) pp 283-291 (1968)
35. Y. Guyot, R. Moncorgé, L.D. Merkle, A. Pinto, B. McIntosh, H. Verdun, "Luminescence properties of Y_2O_3 single crystals doped with Pr^{3+} or Tm^{3+} and codoped with Yb^{3+}, Tb^{3+} or Ho^{3+} ions", Opt. Mater. **5**, pp 127-136 (1996)
36. L. Pauling and M. D. Shappell, Z. Krist. **75**, 128 (1930)
37. W. G. Wyckoff, *Crystals Structures*, 2nd ed. (Interscience, New York, 1964), Vol. 2
38. J. B. Gruber, W. F. Krupke, and J. M. Poindexter "Crystal Field Splitting of Trivalent Thulium and Erbium J Levels in Yttrium Oxide" J. Chem. Phys. **41**, pp 3363-3377 (1964)
39. R. P. Leavitt, J. B. Gruber, N. C. Chang, and C. A. Morrison "Optical spectra, energy levels, and crystal field analysis of tripositive rare earth ions in Y_2O_3. II. NonKramers ions in C_2 sites" J. Chem. Phys. **76**, pp 4775-4788 (1982)
40. W. F. Krupke, "Optical Absorption and Fluorescence Intensities in Several Rare-Earth-Doped Y_2O_3 and LaF_3 Single Crystals" Phys. **145** (1) pp 325-337 (1966)

41. C. A. Morrison, R. P. Leavitt, J. B. Gruber, and N. C. Chang, "Optical spectra, energy levels, and crystal field analysis of tripositive rare earth ions in Y_2O_3. III. Intensities and g values for C_2 sites" J. Chem. Phys. **79**, pp 4758-4763 (1983)
42. L. Fornasiero, "Nd^{3+} - and Tm^{3+} - dotierte sesquioxide," Ph.D. dissertation, Dept. Phys., Univ. Hamburg, Hamburg, Germany, 1999.
43. P. Koopmann, "Thulium- and holmium-doped sesquioxides for 2 μm lasers," Ph.D. dissertation, Dept. Phys., Univ. Hamburg, Hamburg, Germany, 2012
44. W.T. Carnall, P.R. Fields, and K. Rajnak, "Electronic energy levels in the trivalent lanthanides aquo ions. I. Pr^{3+}, Nd^{3+}, Pm^{3+}, Sm^{3+}, Dy^{3+}, Ho^{3+}, Er^{3+} and Tm^{3+}" J. Chem. Phys. **49** (10), 4424-4442 (1968)
45. N. Spector, R. Reisfeld, and I. Boehm, "Eigenstates and radiative transition probabilities for Tm^{3+} ($4f^{12}$) in phosphate and tellurite glasses" Chem. Phys. Lett. **49** (1) 49-53 (1977)
46. B.M. Walsh, N.P. Barnes, and B. Di Bartolo, "Branching ratios, cross sections and radiative lifetimes of rare-earth ions in solids: applications to Tm^{3+} and Ho^{3+} ions in $LiYF_4$", J. Appl. Phys. **83** (5), 2772-2787 (1998)
47. W.F. Krupke and J.B. Gruber, "Optical-absorption intensities of rare-earth ions in crystals: the absorption spectrum of thulium ethylsulfate" Phys. Rev. **139** (6) A2008-A2016 (1965)
48. Y. Nigara, "Measurement of the optical constants of yttrium oxide", Jpn. J. Appl. Phys. **7**, 404-408 (1968)
49. O. Medenbach, D. Dettmar, R. D. Shannon, R. X. Fischer and W. M. Yen, "Refractive index and optical dispersion of rare earth oxides using a small-prism technique", J. Opt. A: Pure Appl. Opt. **3**, pp 174-177 (2001)
50. P. Koopmann, R. Peters, K. Petermann and G. Huber", Crystal growth, spectroscopy, and highly efficient laser operation of thulium-doped Lu_2O_3 around 2 μm" Appl. Phys. B **102**, pp 19-24 (2011)
51. V. Lupei, A. Lupei, C. Gheorghe, A. Ikesue, "Spectroscopic characteristics of Tm^{3+} in Tm and Tm, Nd, Yb:Sc_2O_3 ceramic" J. Lumin. **128**, pp 901–904 (2008)
52. G. Concas, G. Spano, E. Zych and J. Trojan-Piegza, "Nano- and micro-crystalline Lu_2O_3:Eu phosphors: variations in occupancy of C_2 and S_6 sites by Eu^{3+} ions" J. Phys.: Cond. Matter **17**, 2597 (2005)
53. A. Kremenovic, J. Blanusa, B. Antic, P. Colomban, V. Kahlenberg, C. Jovalekic, and J. Dubic, "A Y_2O_3:Yb nanoscale magnet obtained by HEBM: C_{3i}/C_2 site occupancies, size/strain and crystal field levels of Yb^{3+} ions", Nanotech. **18**, 145616 (2007)
54. S. A. Payne, L. L. Chase, L. K. Smith, W. L. Kway, W. F. Krupke, "Infrared Cross-Section Measurements for Crystals Doped with Er^{3+}, Tm^{3+}, and Ho^{3+}," IEEE J. Quantum Electron. **28**, pp 2619–2630 (1992)
55. A. S. Yasyukevich, V. G. Shcherbitskii, V. E. Kisel, A. V. Mandrik, and N. V. Kuleshov, "Integral method of reciprocity in the spectroscopy of laser crystals with impurity centers" J. Appl. Spectr. **71**(2), pp 202-208 (2004)
52. P. Le Boulanger, J.L. Doualan, S. Girard, J. Margerie, and R. Moncorgé, "Excited-state absorption spectroscopy of Er^{3+}-doped $Y_3Al_5O_{12}$, YVO_4, and phosphate glass" Phys. Rev. B 60 (16) pp 11380-11390 (1999)
53. N. Garnier, R. Moncorgé, H. Manaa, E. Descroix, P. Laporte, Y. Guyot, "Excited state absorption of Tm^{3+} doped single crystals at photon-avalanche wavelengths" J. Appl. Phys. **79**, pp 4323-4329 (1996)
54. S. Luo, R. Moncorgé, J.L. Doualan, H. Xu, Z. Cai, C. Labbé, B. Xu, A. Braud, P. Camy, "Simulation of dual-wavelength pumped 3.5 μm CW laser operation of Er:CaF_2 and Er:KY_3F_{10} in waveguide configuration", J. opt. Soc. Am. B **36** (2), pp 275-284 (2019)